APPLIED SCIENCES AND ENGINEERING

Continuous fiberizing by laser melting (Cofiblas): Production of highly flexible glass nanofibers with effectively unlimited length

F. Quintero[1]*, J. Penide[1], A. Riveiro[1], J. del Val[1], R. Comesaña[2], F. Lusquiños[1], J. Pou[1]

The development of nanofibers is expected to foster the creation of outstanding lightweight nanocomposites and flexible and transparent composites for applications such as optoelectronics. However, the reduced length of existing nanofibers and nanotubes limits mechanical strengthening and effective manufacturing. Here, we present an innovative method that produces glass nanofibers with lengths that are, effectively, unlimited by the process. The method uses a combination of a high-power laser with a supersonic gas jet. We describe the experimental setup and the physical processes involved, and, with the aid of a mathematical simulation, identify and discuss the key parameters which determine its distinctive features and feasibility. This method enabled the production of virtually unlimited long, solid, and nonporous glass nanofibers that display outstanding flexibility and could be separately arranged and weaved.

INTRODUCTION

Generating materials with improved structural and physicochemical features and operational performance represents an important and long-standing technological challenge. Synthetic and analytical studies have highlighted potential applications of nanofibers and nanowires in numerous fields, such as lightweight composite materials, energy generation, filtration, chemical sensing, biomedicine, and electronics (*1*–*4*). Early work by Griffith (*5*) has shown that the strength and flexibility of fibers increase significantly with decreasing diameter. The increase in strength is attributed to a reduction in the number of defects, such as vacancies, impurities, and surface scratches, per unit length as the diameter decreases. Furthermore, the gain in flexibility has triggered the design of innovative fiber-based high-performance materials, such as bendable composites and new fabrics. Extensive efforts have been deployed to develop advanced continuous nanofibers, but conventional spinning methods cannot robustly produce fibers thinner than approximately 2 μm (*4*).

The use of nanoscale reinforcements in composites is controversial because it increases the strength of composite materials but not to the extent expected (*6*, *7*). These poor results, which typically occur when using short discontinuous reinforcements, such as carbon nanotubes (*6*) or silica nanoparticles (*7*), may arise from aggregation and inadequate alignment of the reinforcements, as well as insufficient bonding and load transfer at the interfaces. In addition, the quest for improved structural materials should also consider appropriate fracture resistance. In this sense, long macroscopic fibers have proven useful in conventional extrinsic toughening strategies, such as crack deflection and bridging, where they can increase the toughness of brittle materials by composite reinforcing (*8*). However, from the perspective of toughening, the use of short discontinuous reinforcements are not effective to improve the performance of the nanocomposites, as the extrinsic toughening mechanisms are promoted by increasing, not by decreasing, the reinforcement dimensions (*9*). Thanks to their made-to-measure lengths, continuous nanofibers can combine the benefits of macroscopic reinforcements with the assumed advantages of nanoreinforcements, which might lessen all these disadvantages. They would also be simple to manipulate and align during the manufacturing of advanced composites in addition to reducing fabrication cost and health risks (*4*).

Several methods have been developed to generate nanofibers. Electrospinning (ES) is the chosen method to produce polymer nanofibers (*2*). This simple and cost-effective technique can generate ordered and aligned nanofibers that can be collected as yarns or mats (*2*, *10*). Therefore, while polymer microfibers are mainly mass produced by melt spinning, ES is the method of choice to produce polymer fibers of nanometer-size diameters (*2*). Ceramic nanofibers can also be electrospun using a sol-gel precursor, but their fabrication presents some additional limitations. Calcination of the electrospun sol-gel can cause the nanofibers to clump up and form a mat, which cannot be separated, ordered, or woven. Furthermore, their mechanical strength is usually markedly reduced by the residues and porosity induced during calcination (*11*).

Continuous silica fibers are typically downdrawn from a solid preform, which is melted at its tip. These fibers present superior chemical, photochemical, and heat resistance because they retain useful strength characteristics at temperatures up to 1090°C (*12*). Moreover, because of their low density (2.2 g/cm^3), they exhibit the highest specific strength of any pristine glass fiber on record (*12*). High-temperature taper drawing has led to glass nanowires displaying diameters as small as 50 nm and lengths reaching tens of millimeters (*13*). Laser spinning has provided solid, nonporous, and well-defined glass nanofibers with lengths up to several centimeters (*14*) and tailored compositions even from low viscous melts (*15*). However, this process was not continuous; consequently, the nanofibers exhibited substantial but noncustomizable lengths.

Here, we report a laser-based method that produces practically endless, continuous, solid, and separated glass nanofibers from the melt of a solid preform without requiring a crucible. The continuous fiberizing by laser melting and supersonic dragging (Cofiblas) method leads to glass fibers with controlled and uniform diameter, which can be selected in a range of 30 μm down to 300 nm. Unlike laser

[1]Applied Physics Department, Universidade de Vigo, E.E.I., c/ Maxwell s/n, 36310 Vigo, Spain. [2]Department of Materials Engineering, Applied Mechanics and Construction, Universidade de Vigo, E.E.I., c/ Maxwell s/n, 36310 Vigo, Spain.
*Corresponding author. Email: fquintero@uvigo.es

spinning, it achieves total control of the fiber diameter and increases productivity. The resulting continuous pure silica nanofibers are structurally examined, their exceptional flexibility is analyzed and discussed using a set of innovative techniques, and the key parameters of the method are studied and discussed on the basis of the results of the mathematical simulation of the process.

Continuous fiberizing by laser melting and supersonic dragging (Cofiblas), a novel technique

A comprehensive experimental development process combined with predictions obtained by mathematical simulations was adopted. This allowed an accurate control of Cofiblas parameters. Figure 1 shows the experimental layout of Cofiblas. Specifically, Cofiblas comprises an optical system associated with a high-power CO_2 laser and a feeding system connected to a nozzle. In the optical system, a beam splitter divides the laser into two identical laser beams, which are redirected to face each other on the precursor material through a set of mirrors and the beam-shaping system (BSS). This optical system is specifically designed to uniformly irradiate around the preform and precisely adjust the laser irradiance distribution on it; this is crucial because it ensures that the precursor material is adequately heated. The feeding system controls the volume of precursor material flowing from a 600-μm-diameter cylindrical preform using a stepper motor. Last, a de Laval nozzle provides a uniform supersonic air jet flowing coaxially with the filament, which stretches the precursor material to form the nanofibers.

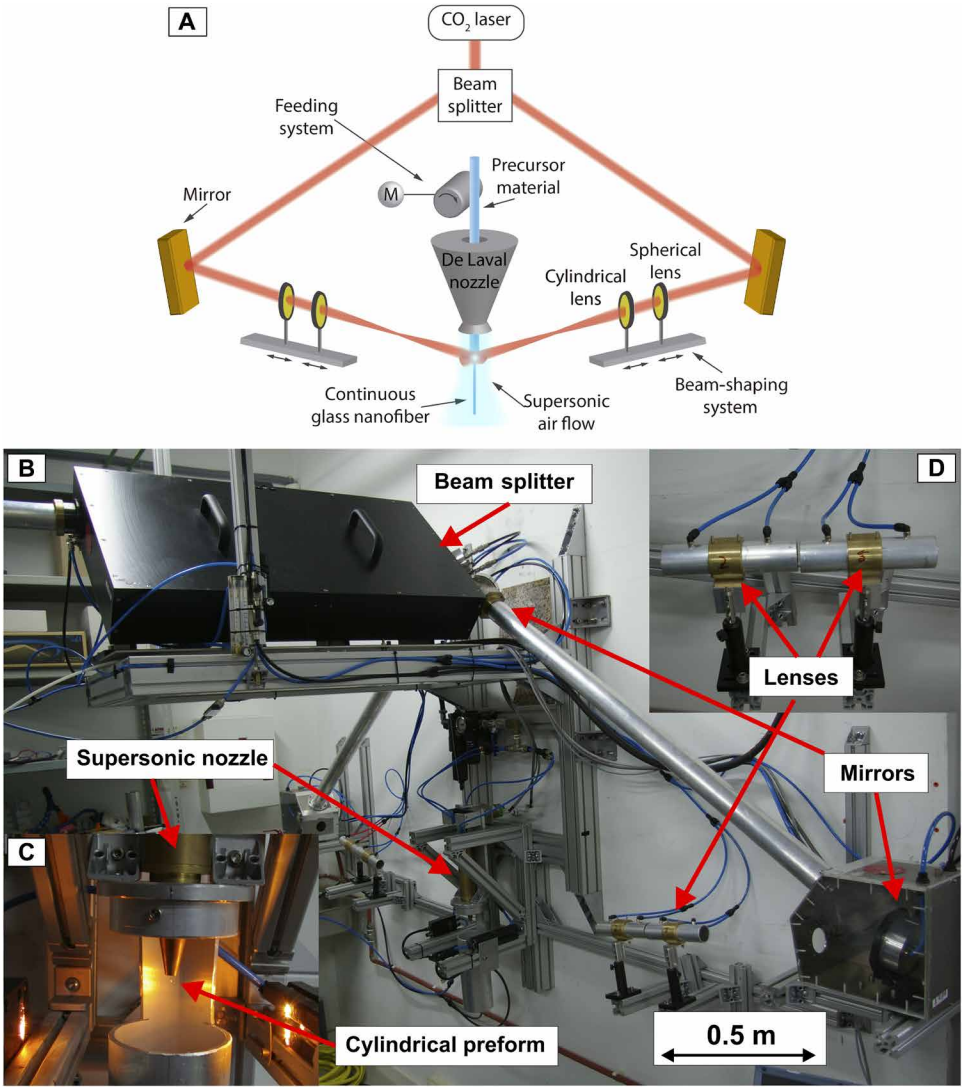

Fig. 1. Experimental setup of Cofiblas system. (**A**) Schematic representation of the setup. A CO_2 laser beam is split into two beams, which are oriented to face each other through a set of mirrors. The beam-shaping system (BSS) is constituted by two spherical and cylindrical lenses. It was specifically designed to change independently the irradiance distribution across two perpendicular axes of the beam cross section. The two beams heat uniformly the precursor material, which gradually melts into a viscous filament. Concurrently, the filament is stretched to form the nanofiber under the supersonic air flow, supplied by a de Laval nozzle, which coaxially surrounds the preform of precursor material. (**B**) Overall view showing the beam splitter, mirrors directing the laser beam toward the preform, the lenses of the BSS, and the Cofiblas-supersonic nozzle with the preform. (**C**) Cofiblas-supersonic nozzle and silica cylindrical preform emerging from the bottom of the feeding system. (**D**) Close-up image of the BSS. The spherical and cylindrical lenses are mounted into a cylindrical holder with assembly alignment and a clean air flow for protection and refrigeration. Photo credit: Joaquín Penide, Universidade de Vigo.

Pure silica was selected as precursor material of Cofiblas because silica nanofibers are expected to show excellent properties; however, pure silica presents a high melting temperature, which hinders the production of silica glass nanofibers by conventional methods. In commercial methods, pure silica is processed at fiber-forming temperatures (approximately 2100°C) (*16*) well above its liquidus temperature of 1713°C (*17*) to avoid devitrification and facilitate stretching by moderate drawing tension. This process must be carried out in special furnaces to obtain fibers with typical diameters above 100 μm (*16*). In contrast, in the Cofiblas technique, the laser beams rapidly heat a very small volume of the high-purity silica precursor until it reaches a temperature above the liquidus point in a crucible-free setup. Both laser beams deliver high energy that leads to substantial temperature gradients. The temperature distribution can be precisely controlled by adjusting the laser beam parameters to obtain the proper viscosity to guarantee filament stability while being stretched by the supersonic jet. Concurrently, the air flow exerts a uniform high tension along the molten material, which is essential for the rapid stretching of the filament.

The essential advantages of Cofiblas compared to other methods are the extremely fast thermal process (full melting and cooling cycle are completed in the order of milliseconds; see Discussion) attained by laser heating, and a large axial stress (maximum tension reached in the filament is estimated around 1 GPa; see Discussion) applied by the supersonic gas jet principally localized at the molten part of the filament. This particular distributed dragging stress avoids the high drawing forces applied by the winding drum of conventional techniques at the thinner part of the solid fiber. The unique combination of both processes guarantees the melt stability against filament rupture by capillary forces, prevents the filament from devitrification, and balances the drawing forces with regard to cohesive forces in the melt. The fulfillment of these conditions is a unique feature of the present method required to obtain continuous glass nanofibers. This is the only method that is able to produce continuous glass fibers 1 m long (with the possibility to produce fibers with lengths not limited by the process) and diameters at nanometer scale. The precise adjustment of the laser irradiance distribution on the filament has demonstrated to be crucial. The BSS consists of two systems of lenses, one set for each laser beam, each one composed of a spherical and a cylindrical lens. It provides an approximately Gaussian irradiance distribution along the axes of the elliptical cross section, with its major axis parallel to the filament.

RESULTS

To optimize the Cofiblas technique, we performed an extensive set of experiments, which we conceived using the design of experiments (DoE) methodology and with help of predictions from the mathematical simulation (see Materials and Methods for details). The optimized Cofiblas process continuously yielded nanofibers with minimum diameters of (370 ± 70) nm (Fig. 2A) from the 600-μm-diameter cylindrical silica preform, which means a 1621-fold average reduction in the diameter. This technique enables the unprecedented continuous production of nonporous and free-standing glass nanofibers. Electron micrographs [Fig. 2, A and B (inset)] also show that the fibers have cylindrical shapes and uniform diameters along their entire length. In addition, they are well defined, which means that, unlike most electrospun fibers, they do not aggregate into mats. The optical micrograph presented in Fig. 2B shows a single fiber with a length of 1 m and a diameter of 2 μm wound parallel around a wooden spool. This picture demonstrates the possibility of processing very long fibers produced by the Cofiblas technique to align and wind them to form a coil. Unfortunately, with the current method of manual collecting and manipulating the as-produced fibers, it was not possible to collect and wind longer or thinner fibers around the wooden spool, despite that much thinner fibers were continuously produced. Future developments should be carried out to improve the collecting and manipulating processes of the fibers to preserve them.

The selective area diffraction pattern of the fiber (Fig. 2C) and the x-ray diffraction analysis (see fig. S3) reveal that all nanofibers are amorphous, proving that devitrification is completely avoided. Scanning electron microscopy (SEM) images (Fig. 2, D and E) show that the nanofibers are produced from the elongation of the preform in two stretching zones. Figure 2E shows details of the second stretching step with the nanofiber still attached to the preform. These stretching zones constitute the two main steps of a stable elongation, which can be kept stationary by properly adjusting the operating conditions. In this way, a continuous nanofiber can be collected at the end of the process at a production rate of 2.6 m/s. These SEM images show a sample obtained when the process was interrupted by turning off the laser beam, demonstrating the stability of the process. As-produced nanofibers were thermally annealed at 700°C for 4 hours to facilitate handling.

Another remarkable result is the extremely high flexibility of the glass nanofibers produced by Cofiblas. Their flexibility was assessed by determining the minimum radius of curvature that these nanofibers are able to withstand before breaking. During these tests, the fibers were entangled in a holder specifically developed and individually bent using the focused ion beam (FIB) field emission gun (FEG)–SEM dual-beam microscope manipulator until they broke. The SEM micrographs showed that 400-nm-diameter nanofibers could be bent to a minimum radius of approximately 10 μm (Figs. 2, F and G).

Young's modulus of the nanofibers was also measured by means of picoindentations with an atomic force microscopy. Several measurements were made along the length and width of the fibers. In particular, three fibers were analyzed, performing 10 measurements on each sample. This procedure gave Young's modulus of (62 ± 16) GPa.

DISCUSSION

From the initial stages of the Cofiblas conceptualization, we developed a mathematical model to get a deeper understanding of the entire process. The simulation oriented the whole process of designing the experimental system to achieve the adequate process parameters by estimating whether the driving forces involved and the thermal evolution of the filament can produce its stable elongation, leading to the continuous nanofiber formation. Furthermore, the estimation of the physical parameters obtained from the mathematical modeling, together with the experimental observation of the process allowed to identify the key features of the Cofiblas method, which make it a unique process capable of producing continuous glass nanofibers.

Complete details of the formulation of the model can be consulted in the Supplementary Materials; notwithstanding, we are discussing here the main findings which aided to explain the performance of this novel method. In the model, we considered a flow, in which the laser-heated cylindrical preform gradually becomes a viscous fluid while being stretched and cooled by the coaxial supersonic gas jet. Then, a one-dimensional flow arises where the preform is progressively

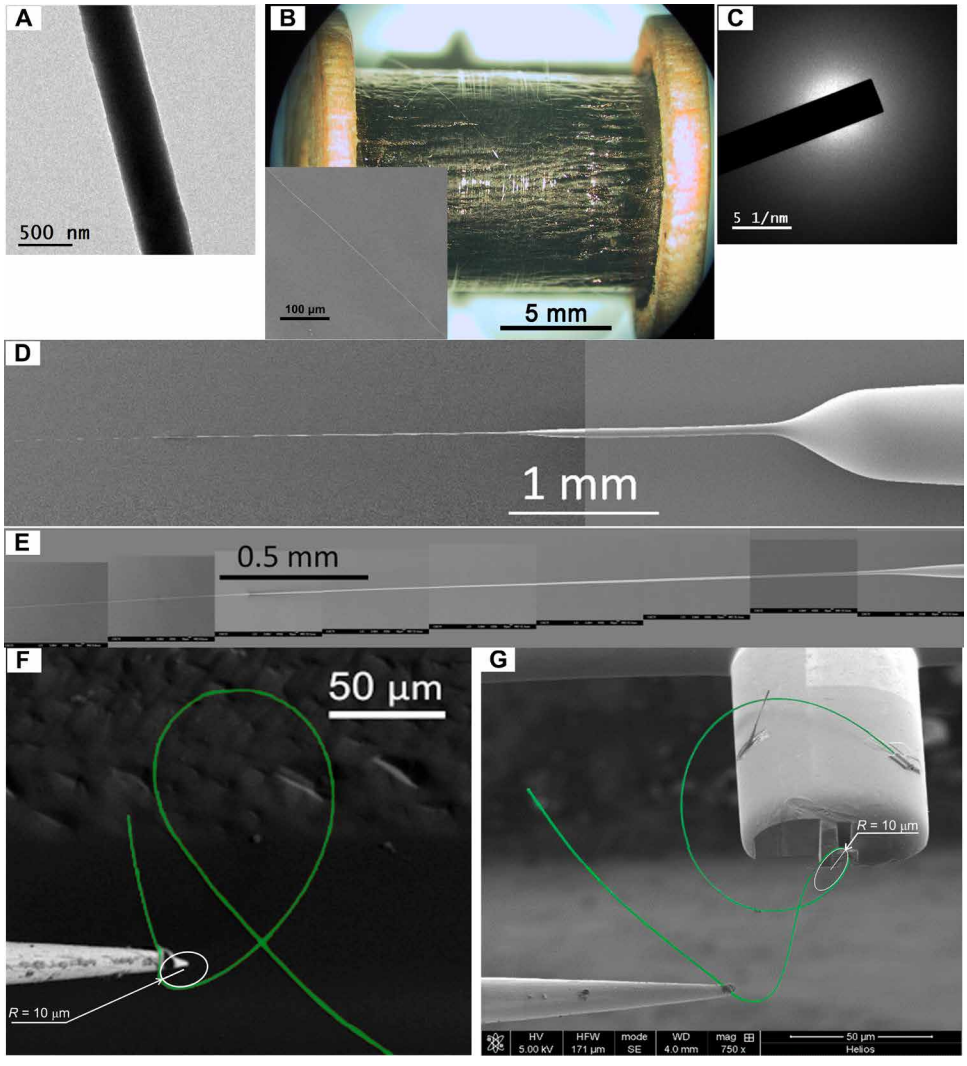

Fig. 2. Micrographs of the filaments produced by Cofiblas: (A) TEM close-up micrograph of a fragment of nanofiber showing a nonporous and smooth fiber surface. (**B**) Wooden spool containing 1-m-long single fiber wound and parallel aligned. Inset: Scanning electron microscopy (SEM) detail of one nanofiber revealing that nanofibers are cylindrical, continuous, and individually separated nonforming mats. (**C**) Selective area diffraction pattern demonstrating that the as-produced fibers are completely amorphous. (**D**) Composite of two SEM images of the cylindrical preform showing two stretching zones. (**E**) Composite of nine SEM images with details of the second stretching step. (**F** and **G**) SEM micrographs of the curvature analysis of glass nanofibers performed in the focused ion beam (FIB). These micrographs were obtained right before the nanofibers fractured when bent using the FIB manipulator. Nanofiber images are colored for clarity, and the ellipses included are perspective drawings of the circumscribed circumferences used to estimate the minimum radius of curvature. Photo credit: Joaquín Penide, Universidade de Vigo.

elongated along its axial direction, z. This elongation reduces the cross-sectional area of the flow while augmenting its axial flow velocity, v_z, although these variables at any point in space are independent of time. Any effect derived from the radial stress and strain components of this uniaxial elongation are negligible; therefore, the flow is irrotational. Hence, the axial flow velocity, the cross-sectional area, the extra stress tensor, and the rate of strain tensor are functions of z only. The total stress is related to the gradient of axial flow velocity, dv_z/dz, using the material constitutive equations to give the differential equation of motion. The material constitutive equation for a Newtonian fluid with viscosity, μ, relates the extra stress tensor, $\boldsymbol{\tau}$, to the extension rate tensor, $\dot{\boldsymbol{\varepsilon}}$, as (*18*)

$$\boldsymbol{\tau} = 2\mu\dot{\boldsymbol{\varepsilon}} \tag{1}$$

Then, considering the boundary condition at the surface of the cylinder, we obtain the axial component of the total stress as a function of the gradient of axial flow

$$T_Z = 3\mu\frac{dv_Z}{dz} - \frac{\sigma}{R} \tag{2}$$

where σ is the surface tension of the fluid filament, and R is its local radius. Substituting this equation in the momentum balance, eq. S5B, we obtain a nonlinear differential equation to solve the gradient of axial flow velocity, which can be subsequently introduced in Eq. 2 to find the total axial stress, an essential parameter to assess the spinnability and performance of the process (*19*).

Molten silica is considered to behave as a perfect Newtonian fluid in many cases, and then, just a temperature dependence of viscosity is modeled using the Arrhenius function. However, one notable

exception is precisely occurring in flows with high strain rates (*20*). In these cases, a model of strain-rate dependence of viscosity should be considered together with the temperature dependence. Specifically, we used the "shear-thinning" model that considers a reduction of the Newtonian viscosity at high strain rates, particularized by our one-dimensional irrotational elongation according to the following equation (*20*)

$$\mu(T,\dot{\varepsilon}_{zz}) = \frac{\mu_N(T)}{1 + 3.5\times10^{-6}\mu_N(T)^{0.76}\frac{dv_Z}{dz}} \quad (3)$$

where $\mu_N(T)$ is the Newtonian viscosity and $\mu(T,\dot{\varepsilon}_{zz})$ is the viscosity modified by the shear-thinning effect expressed as a function of the axial strain rate, $\dot{\varepsilon}_{zz} = dv_z/dz$, this is the viscosity which we used in the calculations.

In addition, the equation of conservation of energy is solved to find the axial derivative of the temperature. This equation is obtained from an energy balance calculated in terms of power for stationary conditions in the control volume formed by an infinitesimal element of the filament. The power lost by convection is evaluated using a mathematical expression obtained experimentally for the melt spinning of polymers (see details in the Supplementary Materials). However, we derived a specific expression to estimate the power absorbed from the laser beam in the control volume, since this power per unit length varies as a function of the z axis position, and this variation was found to be crucial for the success of the process. The variation of the power absorbed from the laser as a function of z varies due to two factors: first, the irradiance distribution on the laser beam along the filament, which must be carefully adjusted with the BSS; second, the filament diameter is also a function of z. To calculate this power per unit length, we first estimate the irradiance of the laser beam at each point, and then we calculate the absorbed power as a function of the beam diameter at each point. Thus, we assume that the irradiance of the beam corresponds to a Gaussian distribution in the direction of the filament axis, z, which is very close to reality. However, for simplicity, we consider a uniform irradiance distribution in the transverse direction to the filament instead. Once the irradiance is expressed as a function of the axial position, the energy absorbed by each unit length of the filament is obtained by estimating the volumetric absorption according to the Beer-Lambert-Bouguer law (*21*). The coefficient of absorption α at the CO_2 laser wavelength strongly depends on temperature (*22*). However, assuming that the regime is stationary in the irradiated volume, this temperature dependence is neglected. Consequently, we estimate a uniform coefficient of absorption for the high temperature reached in the processing volume using (*22*)

$$\alpha = \frac{4\pi\kappa}{\lambda} \quad (4)$$

where κ is the imaginary part of the refractive index of amorphous silica at the wavelength λ. Then, the radiative power absorbed from the laser beam by each unit length of the filament as a function of z, $\frac{\partial \dot{q}_a(z)}{\partial z}$, can be estimated by integrating the following equation along the radial x axis between the boundaries of the filament, $R(z)$ and $-R(z)$

$$\frac{\partial \dot{q}_a(z)}{\partial z} = I_l(z)\int_{-R(z)}^{R(z)}\left(1 - e^{-\alpha\sqrt{R^2(z)-x^2}}\right)dx \quad (5)$$

where $I_l(z)$ is the laser irradiance distribution as a function of z.

Last, the differential form of the equation of continuity gives the variation of the filament radius. Therefore, we obtain a set of three ordinary nonlinear differential equations and several complementary equations, which are described in detail in the Supplementary Materials. We integrated this set of equations numerically using a variable-step solver based on the numerical differentiation formulas. The integration of these equations gives the solution of the main variables as a function of the axial position, and, subsequently, we can calculate the main physical parameters of the process using the former equations. The numerical values of all the parameters used to solve these equations are detailed in the mathematical model in the Supplementary Materials.

During fiber formation, the portion of the laser beam that actually irradiates the precursor material diminishes with the diameter of the melted material (from zone A to zone C in Fig. 3A). When the diameter of the molten filament reaches the micrometric range, the irradiated area corresponds to only a small fraction of the beam cross section. At the beginning of the second stretching zone (zone B), the filament has a diameter around 10 μm, while the width of the laser beam is around 2 mm, and then, the irradiated area corresponds to a fraction of several thousandths of the beam cross section. Therefore, this fraction needs a higher beam irradiance to maintain the temperature necessary for the stretching process. On the other hand, the energy delivered at the stretching starting point (zone A) must remain constant to prevent an excessive and destabilizing temperature rise at this point. The experimental observations and mathematical simulations verify the above-described performance of the optimum optical configuration. Figure 3B shows the silica filament being stretched by Cofiblas operating with the multilens system. The cylindrical preform presented two clear stretching spots, indicating that the BSS generates an irradiance distribution that yields an additional stretching zone necessary to extend the filament elongation down to the nanometer range. Consistently, Fig. 3C shows the distribution of temperature along the filament obtained from the mathematical simulation using a set of parameters, which give a nanofiber with a final diameter of 380 nm. The graph represents a temperature distribution in accordance with the brightness pattern observed in Fig. 3B, and there are two temperature peaks that reproduce the two stretching zones detected experimentally in Fig. 2D. The maximum temperature reached in this particular case was notably low, just 1550°C, which is well below the conventional fiber-forming temperature for pure silica. An alternative simulation, corresponding to a different laser irradiance distribution on the silica filament, predicts a maximum temperature around 1900°C to generate a thinner fiber close to 300 nm. Notwithstanding, further experiments would be required to verify this last estimation, and they are out of the extent of the present work since the optical arrangement to produce such an irradiance distribution would entail an alternative experimental setup. However, the temperature range calculated may be used to estimate a working window. This estimated range of temperatures give a Newtonian viscosity window for the Cofiblas fiberizing process between $10^{7.5}$ Pa·s and $10^{5.1}$ Pa·s. This viscosity range is effectively above the range of spinnability for conventional methods (*19*). Notwithstanding, we must take into account three different facts that can explain the distinctive feasibility of the Cofiblas method: One is the extremely high strain rates in our process, which produce a viscosity reduction due to the mentioned shear-thinning effect (Eq. 3). The effective viscosity can decrease by two orders of magnitude for the estimated gradient of the axial flow,

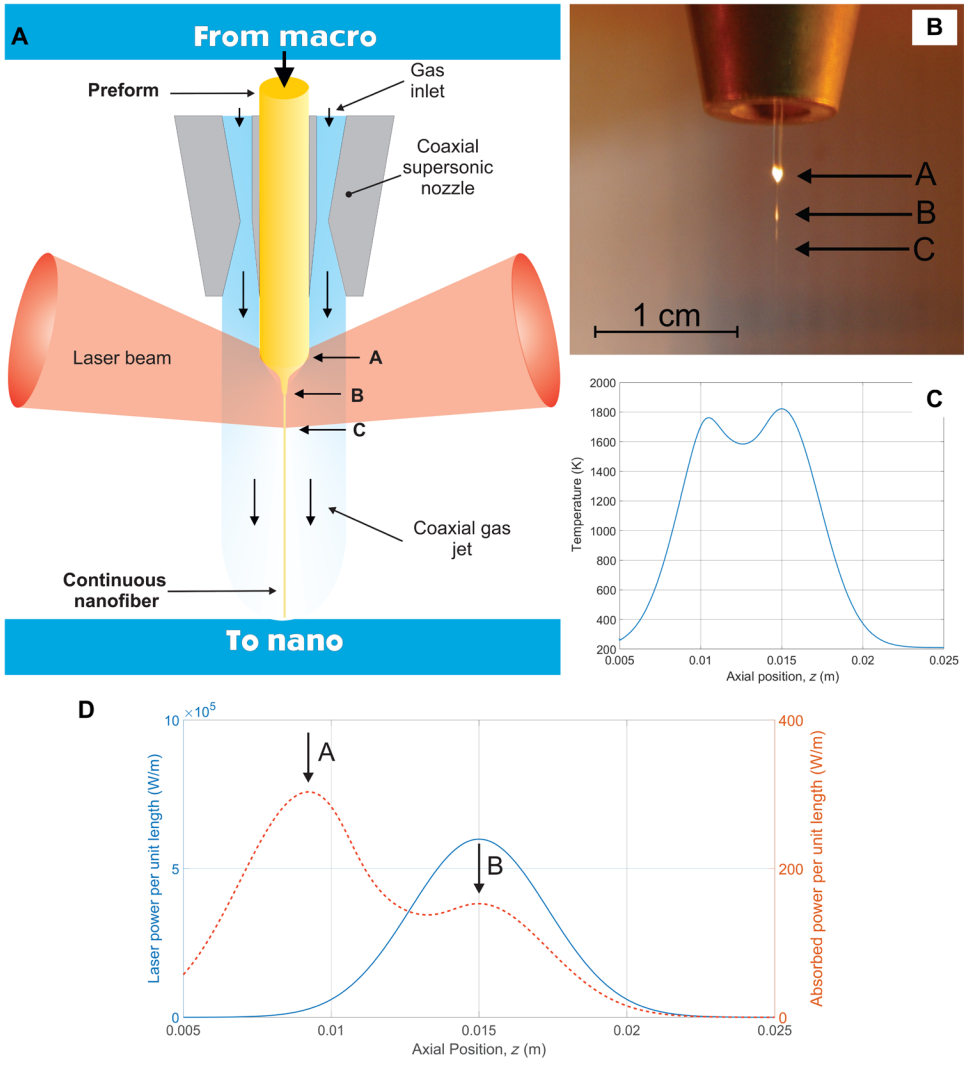

Fig. 3. Experimental and theoretical analysis of the two-points heating and stretching pattern of the filament. (**A**) Schematic representation of the irradiation of the preform by the laser beams. (**B**) Optical photographs of the Cofiblas system during operation showing a detail of the heating and stretching zones of the preform right below the nozzle. The nozzle with the preform of the precursor material is in the upper part. The two laser beams (not visible in this optical image) travel from the right and from the left part of the image and reach the preform from both sides. The arrows point to the approximate position of the zones described in (A). (**C**) Estimated temperature distribution along the silica filament for a simulation producing a continuous fiber with a diameter of 380 nm. (**D**) Comparison between the distribution of the radiative power absorbed from the laser beam per unit length and the irradiance distribution in the incident laser beam. Both graphs (C and D) were obtained from mathematical modeling of the Cofiblas process (see details in the Supplementary Materials). Photo credit: Joaquín Penide, Universidade de Vigo.

which reached values in the range of 100 $s^{-1} < dv_z/dz < 1000\ s^{-1}$. The second difference is the higher total axial tensile stress, which is estimated for the Cofiblas using Eq. 2 to be in the range of 0.1 GPa < T_z < 1 GPa. This is an axial stress around one order of magnitude above the typical values for conventional methods (*23*), thus yielding a feasible spinnability working window. Third, in the Cofiblas method, the axial stress is produced by the gas jet distributed along the part of the filament where the elongation process is produced. In this way, the filament integrity is not compromised by high tension at its thinner and solid section.

We also calculated the laser power absorbed in the filament (Fig. 3D). The maximum signaled as point A in the curve of absorbed laser power corresponds to the first heating zone produced in the preform, which is also experimentally detected in Fig. 3B. It can be observed that this maximum is generated by a moderate irradiance of the laser beam (solid curve in Fig. 3D). These mathematical simulations highlighted an additional absorbed fraction of radiation (zone B) that strongly depends on the irradiance distribution of the laser beam cross section. The zone B in the curve of absorbed power appears in the simulations after a severe reduction of filament diameter [in the micrographs presented in Fig. 2 (D and E), the filament revealed a diameter reduction of the filament preform of 600 μm to around 10 μm at the beginning of zone B], in agreement with experimental verification in Fig. 3B.

Arguably, the most important achievement of the Cofiblas technique lies in its high stability during operation; this facilitates the continuous production of fibers, which means that these fibers are effectively endless. Therefore, the analysis of their stability during elongation is essential to demonstrate the feasibility of the process. The breakup mechanism of a Newtonian flow is typically driven by

surface tension. Elastic or ductile rupture, i.e., a 100% reduction in cross section within a neck caused by a high local stress level (*24*), cannot occur in a pure Newtonian fluid. For mass conservation, the rate at which the minimal cross section of a fluid filament decreases is proportional to the cross section itself multiplied by an axial velocity gradient (see eq. S4B). As long as this gradient is finite, as is to be expected when only finite forces are acting, a decrease in the minimum thickness will be at most exponential, leading to failure only in infinite time. While finite forces cannot induce flow rupture, surface tension is responsible for the eventual breakup. The breakup of the fluid thread arises from instabilities due to interfacial tension in elongational flows of pure viscous filaments (*24*).

Consequently, in the present process, filament stability hinges on the equilibrium between two competing flows: elongational flow and breakup flow (Fig. 4, A to C). Produced by the supersonic air jet, the elongation flow is the only flow that stretches the cylindrical preform to generate the fibers. The breakup flow is driven by the surface tension and tends to interrupt the flow of viscous materials. The relative velocity of these flows determines the final result of Cofiblas, and this velocity depends on the viscosity of the molten

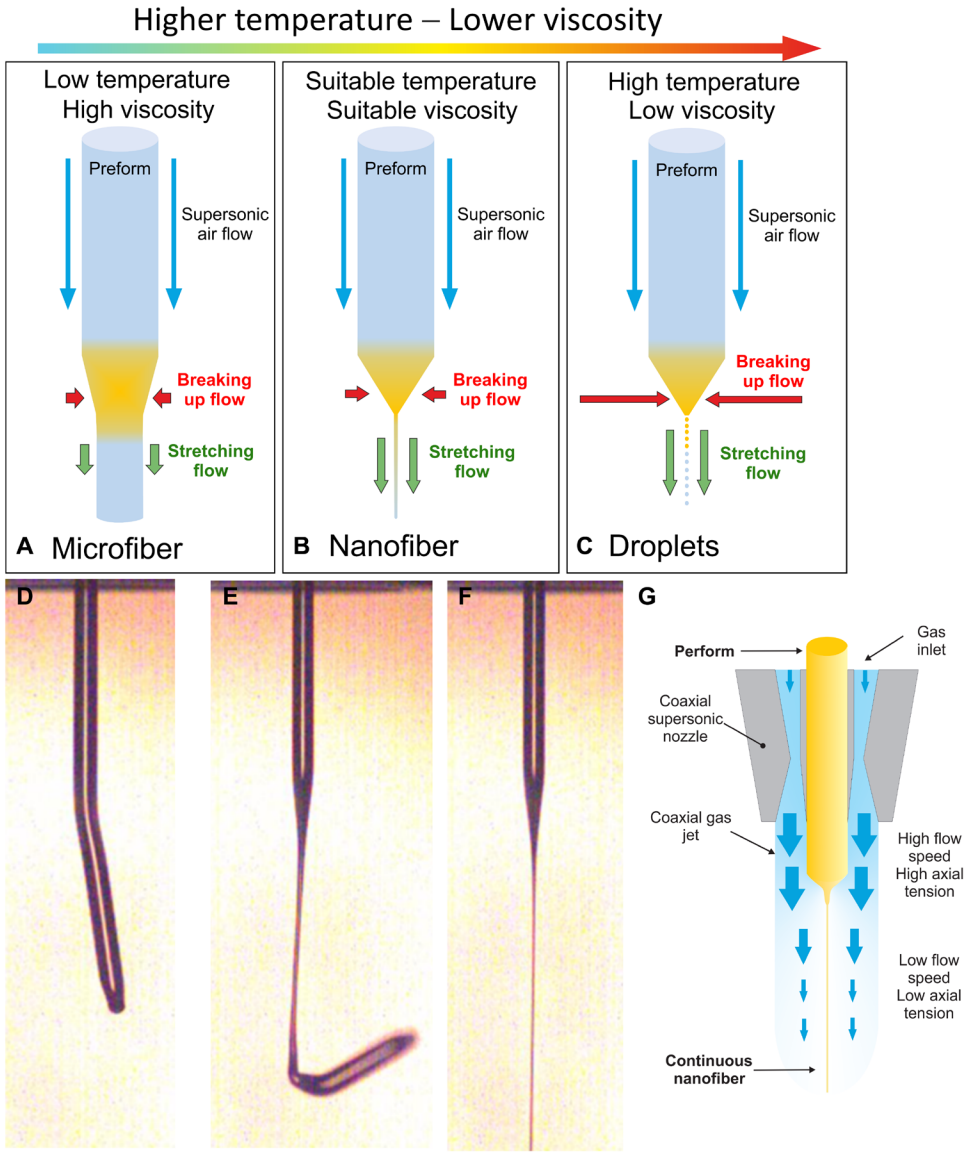

Fig. 4. Experimental and theoretical analysis of the stability of the Cofiblas process. (**A** to **C**) Evolution of the Cofiblas process depending on the temperature and viscosity of the molten material. (**D** to **F**) Image sequence of the preform on the air outlet of the nozzle (which can be seen at the top of the images). These images were taken by a high-speed camera with an exposure time of 1/657,000 s and a recording speed of 3000 frames/s. The preform measures 600 μm in diameter. A high-speed video of the initial transitory instants of the Cofiblas process is shown in the Supplementary Materials. (**G**) Schematic representation of the dragging stress exerted by the supersonic gas jet. Close to the nozzle outlet, the gas flow speed reaches its maximum value and also the drag stress, and consequently, the total axial tensile stress reaches its highest value as well. As the gas jet expands against the surrounding atmosphere and the flow becomes more turbulent, the flow speed reduces; therefore, the axial tensile stress decreases equally. Photo credit: Joaquín Penide, Universidade de Vigo.

fluid, which is, in turn, a function of temperature. If the viscosity is too high (Fig. 4A), then both flows are very slow, and a fiber is formed but with a large diameter. If the viscosity is in the appropriate range, then the elongational flow is fast enough to produce nanofibers, while the breakup flow is not too fast to section the fluid filament before the nanofiber is formed (Fig. 4B). In contrast, if the viscosity is too low (Fig. 4C), then the breakup flow is too fast and the fluid filament breaks before the nanofiber forms. The classification of the low or high viscosity ranges are intrinsically relative and depend on the main parameters of the process, since they are defined by the balance between elongational and capillary forces. Therefore, the Cofiblas system must guarantee a proper control over the processing parameters and conditions to work within the range of viscosities that lead to continuous glass nanofibers.

The stability of the filament against rupture by surface tension can be modeled as an equilibrium between the capillary forces and the viscosity, which mitigates instabilities in the filament. The estimations presented in the section of the Supplementary Materials showing the results of the mathematical calculations (see eqs. S35A, S35B, S36A, and S36B) indicate that the classical approximation based on the Rayleigh model of wave formation (*24*) is the most suitable one. Therefore, the jet lifetime (*12*), t_L, was estimated for the most adverse conditions, which correspond to the state of minimum viscosity or maximum calculated temperature.

$$t_L = 14\left(\sqrt{\frac{8\rho R^3}{\sigma}} + \frac{6R\mu}{\sigma}\right) \quad (6)$$

$$t_L(1550°C) = 4.55 \times 10^3\,s; t_L(1900°C) = 18.1\,s$$

This jet lifetime time can provide an approximated assessment of stability when compared to characteristic time of elongation, i.e., the time spent by the fluid at high temperature. This comparison revealed that, under optimized operating conditions, the jet lifetime is several orders of magnitude higher than the residence time of the filament material in the fluid state. The estimated flow rate in the zone of maximum temperature ranged between 0.5 and 3 m/s, suggesting that the fluid takes approximately 5 ms to complete the filament elongation. Consequently, the maximum calculated temperature was well within the conditions of stability against rupture of the filament by surface tension.

Furthermore, in the Cofiblas method, the axial stress is produced by the gas jet distributed along the part of the filament where the elongation process is produced. It can be observed in the photograms sequence presented in the Fig. 4 (D to F) that the lower and thinner part of the filament oscillates practically free of axial tension, which is also in accordance with the results of the mathematical simulation. This allows applying a higher tension than in conventional processes where the tension is applied by a winding drum at the end of the filament. In the conventional processes, the application of a high drawing force in the thinner part of the filament may compromise the integrity of the solid fiber, which can break if its ultimate strength is surpassed. On the contrary, in the Cofiblas method, the solid nanofiber is free of the high tension produced by the gas jet, since the highest total axial tensile stress is applied where the gas flow speed reaches its maximum regime, close to the nozzle outlet, coinciding with the fluid state of the filament (see Fig. 4G). Conversely, as the gas jet evolves against the surrounding atmosphere, it undergoes a further expansion and an increase of the turbulent regime. Consequently, the axial tensile stress exerted on the filament decreases, since the gas drag stress cuts down.

Consequently, we hypothesize that the higher drawing stress and strain rate applied in the Cofiblas process compared to other spinning processes allows the elongation of a filament with higher viscosity, subsequently increasing its stability. Conversely, the lower limit of the temperature range is below the liquidus temperature of silica; notwithstanding, the Cofiblas method can successfully generate amorphous fibers because the process is so fast that it avoids the onset of crystallization. Actually, an estimation of the cooling rate yields a value around 2×10^5°C/s, which is of the same order of magnitude as that estimated for a rotary spinning (*25*). This high cooling rate can effectively produce amorphous fibers without devitrification.

The radius of curvature of 10 μm observed just before the fiber break in the experiments performed with the FIB (Fig. 2, F and G) revealed a remarkable flexibility. This outstanding flexibility can be stressed by comparison with different long glass fibers continuously produced with conventional methods. We estimated the minimum radius of curvature for the thinnest fibers of silica, E-glass and S-glass continuously produced, assuming that the fibers behave as an isotropic elastic rod (*26*) and considering the best mechanical properties reported (*12*). The minimum radius of curvature obtained for all these fibers are between 90 and 200 μm, around one order of magnitude higher than the present case (see the Supplementary Materials for details). This exceptional result, which is presumably attributed to their reduced diameter and, consequently, is an structural property, can be related to the intrinsic mechanical properties of the fibers to discuss its consistency. Young's modulus measured by the picoindentation analyses gave an average value of (62 ± 16) GPa, which gives a reduction of 14% compared to annealed bulk silica (≈72GPa) (*27*, *28*). The reason for this reduction of the modulus may be explained by a change in the intermediate-range order of the structure of silica induced by the elongation process. It is well known that the mechanical properties of glass fibers differ from the bulk glass because axial stress applied to the viscous filament during fiber drawing creates structural anisotropy (*29*, *30*). Conventional drawing methods (using pulling stresses up to 150 MPa) (*23*) can reduce the elastic modulus of glass fibers by as much as 10% (*29*). Moreover, the distortion of the silica structure under higher applied compression stresses, 26.2 GPa at 25°C (*27*) or 8 GPa at 1100°C (*28*), can cause a much higher variation in Young's modulus of silica (60 and 71% respectively). Therefore, during the Cofiblas process, the high axial tensile stress applied to the filament at high temperature (we estimated a drawing stress in the order of 1 GPa at a temperature exceeding 1300°C) may anisotropically distort the silica structure, leading to a reduction in Young's modulus.

The minimum radius of curvature of a filament, R_{min}, can be related to Young's modulus and the strength of the material as (*26*)

$$R_{min} = \frac{ER}{\tau_{max}} \quad (7)$$

where E is the Young's modulus, and τ_{max} is the ultimate strength of the nanofiber. Therefore, taking Young's modulus measured by the picoindentation experiments and the minimum radius of curvature of 10 μm for the 400-nm-diameter fiber, we obtain an ultimate strength of the nanofiber of (1.24 ± 0.32) GPa, which is in the range expected for silica fibers (*12*, *31*). Future work is ongoing to further and more detailed analyze the mechanical properties of the nanofibers.

Table 1. Parameters varied in the experiments performed for optimizing the Cofiblas process.

	DoE1	DoE2	DoE3
L (mm)	20–30	30–45	20–30
A ($\pi 4^{-1}$ mm^2)	40–60	90–180	120–180
$v_z(0)$ (μm s^{-1})	100–500	1–4	1–4
v_a (m s^{-1})	420	420	490
T_a (°C)	−60	−60	−90
P_l (W)	420–3500	450–3500	350–3500
D (μm)	34–7.5	0.37–5.6	0.7–3.8

In summary, continuous laser supersonic fiberizing technique enabled the unprecedented production of glass nanofibers as thin as 370 nm in diameter, with virtually unlimited length. The solid and nonporous nanofibers displayed outstanding flexibility, resting on their very thin diameter and mechanical features equivalent to conventional glass fibers. These findings represent a group of synergetic advantages that can expand the applications of glass fibers. Because of their exceptional characteristics of made-to-measure length, solid nonporous, and freestanding nature, together with good mechanical properties, nanofibers produced by Cofiblas could be used as mechanical reinforcements of nanocomposites. The flexibility and visible-light transparency of these fibers open new possibilities for the generation of ultraflexible composites applicable to optoelectronic flexible devices, high-performance textiles, and elastomers. This proof-of-concept study can be easily extended to other glass compositions (such as bioglasses and high strength glasses) by carefully adjusting the operating conditions. The Cofiblas technique can also readily achieve the high fiber-forming temperature in addition to extremely fast elongation and cooling, which facilitates the fabrication of high-performance nanofibers from compositions with elevated liquidus temperatures without devitrification.

MATERIALS AND METHODS

Experimental setup and DoE

Optram PWF pure silica fibers (CeramOptec, Germany) displaying a diameter of 600 μm were used as precursor material. The silicon cladding and the nylon jacket of the original silica optical fibers were manually removed before use. The precursor material movement was controlled by a stepper motor (Maxon EC45).

Figure 1 shows the experimental setup for the Cofiblas process. A CO_2 laser (Rofin) working at a wavelength of 10.6 μm with a maximum output power of 3.5 KW was divided into two laser beams using a 50/50 beam splitter (Rofin). Both laser beams were redirected to face each other at the outlet of a de Laval nozzle on the silica preform and at an angle of 80° with respect to the longitudinal axis of the preform. The irradiance distribution on the preform was adjusted using the BSS comprising ZnSe spherical and cylindrical lenses with focal distances of 750 and 267 mm, respectively. The de Laval nozzle generated a supersonic air jet that surrounded the preform and axially flowed along the entire length of the filament. This nozzle was specially designed to reduce turbulence and instabilities along the filament and to maximize the dragging force that stretches the molten material (more details are provided in the Supplementary Materials).

Because of the elevated number of factors that influence the Cofiblas process, we used the DoE methodology to study the influence of a number of parameters and optical configurations on the stability of the process and on the features of the fibers produced. Three different full factorial DoEs, each one with three factors in two levels were planned after a series of preliminary experiments. Specifically, two of the factors were related with the irradiance distribution of the laser beam on the filament. We varied the irradiance distribution by changing the cross section of the laser beam on the filament. The BSS makes it possible to change independently both axes of the elliptical cross section of the laser beam by varying the working distances of the spherical and cylindrical lenses with respect to the filament. In the DoE, we used two parameters representing the irradiance distribution: the length of the mayor axis, L, and area of the elliptical cross section, A. The third factor of the DoE is the feeding speed of the preform to the nozzle, which is equivalent to the axial flow velocity of the filament at the beginning of the elongation, $v_z(0)$. On the other hand, in two sets of experiments, we used the nozzle designed for low air pressure and Mach 1.5, while in the DoE3, we used the de Laval nozzle designed for higher air pressure and Mach 1.8, which involves a different air flow speed, v_a, and temperature, T_a, in the supersonic jet (both were estimated theoretically assuming an isoentropic expansion in the nozzle). Every experiment was performed with the maximum laser power, P_l, that led to stable operating conditions to generate continuous fibers. In Table 1, we show in detail the ranges of parameters for each set of experiments, together with the average of the diameters (D) measured for the resulting continuous fibers obtained in stable functioning (last line of Table 1).

This study highlighted the following trend: An increase in the spot size along the filament axis and a reduction in the feeding speed lead to fibers with lower diameters. In particular, continuous 370-nm-diameter nanofibers were obtained at a feeding speed of 1 μm/s using 1750-W laser power distributed over an elliptical spot with a major axis of 30 mm and a minor axis of 2 mm. As a final step, the as-produced nanofibers were thermally treated at 700°C for 4 hours in a BWF 12/13 furnace (Carbolite) under a flux of dry air.

Morphological and structural analyses of the fibers

The morphology of the fibers was characterized using a field-emission SEM (JEOL JSM-6700F) and transmission electron microscopy (JEOL JEM-2010 FEG). The as-produced fibers were deposited on carbon adhesive discs for SEM imaging and analyzed without coating. Structural analyses of the fibers were carried out by selective area diffraction pattern in the TEM and by x-ray diffraction.

Mechanical properties

The flexibility of the fibers was assessed using the Omniprobe nanomanipulator of the FEI Helios NanoLab FIB FEG-SEM dual-beam microscope. In each test, a single fiber with a diameter of 400 nm was entangled in a holder specifically shaped by ion milling and individually bent using the FIB manipulator until it broke. A series of successive micrographs were taken until the rupture of the filament occurs, and then, the flexibility of the fiber was estimated by measuring the minimum radius of curvature from the last micrograph taken.

Young's modulus of the nanofibers was also measured by means of atomic force microscopy (NanoWizard 3, JPK Instruments). Picoindentations were made along the length and width of the fibers. Mica substrates (0.21-mm-thick grade V1; TED PELLA, INC.) were

used to fix the nanofibers to be measured. To maximize the adhesion of the nanofibers, a drop of 0.5-mg solution of poly-L-lysine (CAS 25988-63-0) in 1 ml of deionized water was placed on the substrate, allowing 15 min to dry. It was then washed with a solution of NaCl (0.15 M) to activate the charges of the poly-L-lysine and lastly dried with N_2. Last, the nanofibers were deposited on the mica substrate. A tip of 12.00-nm radius and paraboloid shape was used to perform the picoindentations.

SUPPLEMENTARY MATERIALS

Supplementary material for this article is available at http://advances.sciencemag.org/cgi/content/full/6/6/eaax7210/DC1

Section S1. Supersonic nozzle
Section S2. Mathematical formulation of the model
Section S3. High-speed video analysis of the Cofiblas process
Section S4. X-ray diffraction analysis
Section S5. SEM micrographs
Section S6. Fibers flexibility assessment
Fig. S1. Cross-sectional image of the supersonic nozzle used in the Cofiblas system.
Fig. S2. Schematic representation of a differential element, with length, *dz*, of the filament which is being elongated.
Fig. S3. X-ray diffraction spectra of thermally treated silica nanofibers produced by Cofiblas.
Fig. S4. Original SEM micrographs used to assemble the composite of the filament presented in Fig. 2 (D and E).
Table S1. Parameters used to calculate the Newtonian viscosity of molten silica as a function of temperature (*33*).
Table S2. Parameters used to solve the set of differential equations.
Table S3. Initial conditions of the Cofiblas process.
Movie S1. High-speed video showing the initial transitory states of the Cofiblas process and a representative excerpt of the stationary state of the continuous stretching process.
References (*32*–*40*)

REFERENCES AND NOTES

1. L. Persano, A. Camposeo, D. Pisignano, Active polymer nanofibers for photonics, electronics, energy generation and micromechanics. *Prog. Polym. Sci.* **43**, 48–95 (2015).
2. Kenry, C. T. Lim, Nanofiber technology: Current status and emerging developments. *Prog. Polym. Sci.* **70**, 1–17 (2017).
3. C. González, J. J. Vilatela, J. M. Molina-Aldareguía, C. S. Lopes, J. LLorca, Structural composites for multifunctional applications: Current challenges and future trends. *Prog. Mater. Sci.* **89**, 194–251 (2017).
4. Y. A. Dzenis, Spinning Continuous Fibers for Nanotechnology. *Science* **304**, 1917–1919 (2004).
5. A. A. Griffith, The Phenomena o f Rupture and Flow in Solids. *Philos. Trans. R. Soc. A* **221**, 163–198 (1920).
6. Y. Dzenis, Structural nanocomposites. *Science* **319**, 419–420 (2008).
7. S. Mallakpour, M. Naghdi, Polymer/SiO_2 nanocomposites: Production and applications. *Prog. Mater. Sci.* **97**, 409–447 (2018).
8. R. O. Ritchie, The conflicts between strength and toughness. *Nat. Mater.* **10**, 817–822 (2011).
9. M. E. Launey, R. O. Ritchie, On the fracture toughness of advanced materials. *Adv. Mater.* **21**, 2103–2110 (2009).
10. S. Thenmozhi, N. Dharmaraj, K. Kadirvelu, H. Y. Kim, Electrospun nanofibers: New generation materials for advanced applications. *Mater. Sci. Eng. B* **217**, 36–48 (2017).
11. Y. Dai, W. Liu, E. Formo, Y. Sun, Y. Xia, Ceramic nanofibers fabricated by electrospinning and their applications in catalysis, environmental science, and energy technology. *Polym. Adv. Technol.* **22**, 326–338 (2011).
12. F. T. Wallenberger, in *Fiberglass and Glass Technology: Energy-Friendly Compositions and Applications*, F. T. Wallenberger, P. A. Bingham, Eds. (Springer US, 2010), pp. 3–90.
13. L. Tong, R. R. Gattass, J. B. Ashcom, S. He, J. Lou, M. Shen, I. Maxwell, E. Mazur, Subwavelength-diameter silica wires for low-loss optical wave guiding. *Nature* **426**, 816–819 (2003).
14. F. Quintero, A. B. Mann, J. Pou, F. Lusquiños, A. Riveiro, Rapid production of ultralong amorphous ceramic nanofibers by laser spinning. *Appl. Phys. Lett.* **90**, 153109 (2007).
15. F. Quintero, Ó. Dieste, J. Penide, F. Lusquiños, A. Riveiro, J. Pou, Nonconventional production of glass nanofibers by laser spinning. *J. Am. Ceram. Soc.* **97**, 3116–3121 (2014).
16. H. D. Ackler, J. B. MacChesney, in *Advanced Inorganic Fibers: Processes, Structures, Properties, Applications*, F. T. Wallenberger, Ed. (Kluwer Academic Publishers, 2000), p. 192.
17. W. D. Kingery, H. K. Bowen, D. R. Uhlmann, *Introduction to Ceramics* (John Wiley & Sons, ed. 2, 1976).
18. C. J. S. Petrie, *Elongational Flows. Aspects of the Behaviour of Model Elasticoviscous Fluids* (Pitman, 1979).
19. Y. Yue, Q. Zheng, Fiber spinnability of glass melts. *Int. J. Appl. Glas. Sci.* **8**, 37–47 (2017).
20. J. H. Simmons, What is so exciting about non-linear viscous flow in glass, molecular dynamics simulations of brittle fracture and semiconductor-glass quantum composites. *J. Alloys Compd.* **239**, 1–15 (1996).
21. D. Bäuerle, *Laser Processing and Chemistry* (Springer-Verlag, ed. 4, 2011).
22. J. Zhao, J. Sullivan, J. Zayac, T. D. Bennett, Structural modification of silica glass by laser scanning. *J. Appl. Phys.* **95**, 5475–5482 (2004).
23. J. Murach, R. Brückner, Preparation and structure-sensitive investigations on silica glass fibers. *J. Non-Cryst. Solids* **211**, 250–261 (1997).
24. J. Eggers, Nonlinear dynamics and breakup of free-surface flows. *Rev. Mod. Phys.* **69**, 865–930 (1997).
25. Y. Zhang, Y. Vulfson, Q. Zheng, J. Luo, S. H. Kim, Y. Yue, Impact of fiberizing method on physical properties of glass wool fibers. *J. Non-Cryst. Solids* **476**, 122–127 (2017).
26. G. Stan, S. Krylyuk, A. V. Davydov, R. F. Cook, Bending manipulation and measurements of fracture strength of silicon and oxidized silicon nanowires by atomic force microscopy. *J. Mater. Res.* **27**, 562–570 (2012).
27. T. Deschamps, J. Margueritat, C. Martinet, A. Mermet, B. Champagnon, Elastic moduli of permanently densified silica glasses. *Sci. Rep.* **4**, 7193 (2014).
28. M. Guerette, M. R. Ackerson, J. Thomas, F. Yuan, E. B. Watson, D. Walker, L. Huang, Structure and properties of silica glass densified in cold compression and hot compression. *Sci. Rep.* **5**, 15343 (2015).
29. R. L. Hausrath, A. V Longobardo, in *Fiberglass and Glass Technology: Energy-Friendly Compositions and Applications*, F. T. Wallenberger, P. A. Bingham, Eds. (Springer US, 2010), pp. 197–228.
30. M. D. Lund, Y. Yue, Impact of drawing stress on the tensile strength of oxide glass fibers. *J. Am. Ceram. Soc.* **93**, 3236–3243 (2010).
31. V. E. Khazanov, Y. Kolesov, N. N. Trofimov, in *Fibre Science and Technology*, V. I. Kostikov, Ed. (Springer, 1995), pp. 15–230.
32. R. Beyreuther, H. Brüning, *Dynamics of Fibre Formation and Processing* (Springer-Verlag, 2007), p. 50.
33. N. P. Bansal, R. H. Doremus, *Handbook of glass properties* (Academic Press, 1986), p. 14.
34. M. Matsui, Air Drag on a Continuous Filament in Melt Spinning. *J. Rheol.* **20**, 465–473 (1976).
35. B. Majumdar, R. L. Shambaugh, Air drag on filaments in the melt blowing process. *J. Rheol.* **34**, 591–601 (1990).
36. S. Kase, T. Matsuo, Studies on Melt Spinning. I. Fundamental Equations on the Dynamics of Melt Spinning. *J. Polym. Sci. A* **3**, 2541–2554 (1965).
37. A. D. McLachlan, F. P. Meyer, Temperature dependence of the extinction coefficient of fused silica for CO_2 laser wavelengths. *Appl. Opt.* **26**, 1728–1731 (1987).
38. D. H. Peregrine, G. Shoker, A. Symon, The bifurcation of liquid bridges. *J. Fluid Mech.* **212**, 25–39 (1990).
39. A. K. Varshneya, *Fundamentals of Inorganic Glasses* (Academic Press, 1994), p. 151.
40. REFPROP. NIST Reference Fluid Thermodynamic and Transport Properties Database (REFPROP): Version 7.0.

Acknowledgments: We acknowledge the help of J. L. Fernández with the design of the BSS and A. Abalde with the construction of the experimental system. J. Molina from IMDEA-Materials and A. Durán from ICV-CSIC for fruitful discussion. R. A. Pires and R.L. Reis for their help with AFM measurements. Technical staff of CACTI at University of Vigo is also acknowledged by their help with the characterization of some samples. **Funding:** This work was partially funded by the EU research project Bluehuman (EAPA_151/2016 Interreg Atlantic Area), Government of Spain [PGC2018-094900-B-I00 (MCIU/AEI/FEDER, UE)] and by Xunta de Galicia (ED431C 2019/23), and Plan I2C Grant Program (ED481B 2016/047-0, ED481D 2017/010). **Author contributions:** F.Q. and J.Po. designed the study. F.Q., J.Pe., and J.Po. developed the experimental setup and the discussion of the results. J.Pe., A.R., and J.d.V. performed all laser experiments. J.Pe., R.C., and F.L. carried out the morphological characterization of the samples. F.Q., J.Pe., and J.Po. write the manuscript with the input from all other authors. **Competing interests:** The authors are inventors on a patent application related to this work filed by the University of Vigo (no. WO2017077158-A1, filed on 11 May 2017). The authors declare that they have no other competing interests. **Data and materials availability:** All data needed to evaluate the conclusions in the paper are present in the paper and/or the Supplementary Materials. Additional data related to this paper may be requested from the authors.

Submitted 17 April 2019
Accepted 25 November 2019
Published 7 February 2020
10.1126/sciadv.aax7210

Citation: F. Quintero, J. Penide, A. Riveiro, J. del Val, R. Comesaña, F. Lusquiños, J. Pou, Continuous fiberizing by laser melting (Cofiblas): Production of highly flexible glass nanofibers with effectively unlimited length. *Sci. Adv.* **6**, eaax7210 (2020).

ScienceAdvances

Continuous fiberizing by laser melting (Cofiblas): Production of highly flexible glass nanofibers with effectively unlimited length

F. QuinteroJ. PenideA. RiveiroJ. del ValR. ComesañaF. LusquiñosJ. Pou

Sci. Adv., 6 (6), eaax7210. • DOI: 10.1126/sciadv.aax7210